Spin flop and crystalline anisotropic magnetoresistance in CuMnAs

M. Wang,[1] C. Andrews,[1] S. Reimers,[1,2] O. J. Amin,[1] P. Wadley,[1] R. P. Campion,[1] S. F. Poole,[1] J. Felton,[1]
K. W. Edmonds,[1,*] B. L. Gallagher,[1] A. W. Rushforth,[1] O. Makarovsky,[1] K. Gas,[3] M. Sawicki,[3] D. Kriegner,[4]
J. Zubáč,[4,5] K. Olejník,[4] V. Novák,[4] T. Jungwirth,[4,1] M. Shahrokhvand,[6] U. Zeitler,[6] S. S. Dhesi,[2] and F. Maccherozzi[2]

[1]*School of Physics and Astronomy, University of Nottingham, University Park, Nottingham NG7 2RD, United Kingdom*
[2]*Diamond Light Source, Harwell Science and Innovation Campus, Didcot OX11 0DE, United Kingdom*
[3]*Institute of Physics, Polish Academy of Sciences, Aleja Lotnikow 32/46, PL-02668 Warsaw, Poland*
[4]*Institute of Physics, Czech Academy of Sciences, Cukrovarnická 10, 162 00 Praha 6, Czech Republic*
[5]*Faculty of Mathematics and Physics, Charles University, Ke Karlovu 3, 121 16 Prague 2, Czech Republic*
[6]*High Field Magnet Laboratory (HFML-EMFL), Radboud University, Toernooiveld 7, 6525ED Nijmegen, The Netherlands*

We report magnetic-field-induced rotation of the antiferromagnetic Néel vector in epitaxial CuMnAs thin films. First, using soft x-ray magnetic linear dichroism spectroscopy as well as magnetometry, we demonstrate spin-flop switching and continuous spin reorientation in films with uniaxial and biaxial magnetic anisotropies, respectively, for applied magnetic fields of the order of 2 T. The remnant antiferromagnetic domain configurations are determined using x-ray photoemission electron microscopy. Next, we show that the Néel vector reorientations are manifested in the longitudinal and transverse anisotropic magnetoresistance. Dependencies of the electrical resistance on the orientation of the Néel vector with respect to both the electrical current direction and the crystal symmetry are identified, including a weak fourth-order term evident at high magnetic fields. The results provide characterization of key parameters including the anisotropic magnetoresistance coefficients, magnetocrystalline anisotropy, and spin-flop field in epitaxial films of tetragonal CuMnAs, a candidate material for antiferromagnetic spintronics.

I. INTRODUCTION

In antiferromagnetic (AF) materials, the atomic magnetic moments alternate in direction to produce zero net magnetization. The consequent absence of magnetic stray fields and relative insensitivity to external fields offer advantages for certain memory applications [1,2], but also pose a challenge for the writing and reading of information. Recent works have shown that electric currents can be used to rotate the AF spin axis in crystalline materials, including CuMnAs and Mn$_2$Au, where the spin sublattices are space-inversion partners [3–10]. The spin rotation results in an anisotropic magnetoresistance (AMR) effect where the resistance depends on the relative orientation of the spin axis and the current direction.

A collinear AF material is characterized by a Néel vector, $\mathbf{L} = (\mathbf{m_1} - \mathbf{m_2})$, where $\mathbf{m_1}$ and $\mathbf{m_2}$ are the magnetizations of each spin sublattice. An external magnetic field, H, applied perpendicular to $\mathbf{L}$ competes against the strong internal exchange field H_e which couples the sublattices. As a result, a canting of the magnetic moments into the field direction occurs, resulting in a small net magnetization, $\mathbf{M} = (\mathbf{m_1} + \mathbf{m_2})$, when $H \ll H_e$. A more significant reorientation occurs at the so-called spin-flop transition, from an AF state with $\mathbf{L}$ aligned parallel to the external field, to a state with $\mathbf{L}$ perpendicular, but with individual moments canted into the field direction. This is detected as a steplike increase in the magnetic susceptibility in bulk materials with uniaxial anisotropy, but is hard to detect in thin films due to the typically very small canting angle leading to a very weak magnetic signal.

AMR in AF materials has been explored only recently [11–21]. In hexagonal MnTe films, a $\cos 2\theta$ dependence on the angle θ between the current and the external field was demonstrated, due to the spin-flop rotation of the Néel vector [15]. Studies of the canted AF semiconductor Sr$_2$IrO$_4$ have shown a crystalline contribution to AMR, with fourfold symmetry, originating from changes in the equilibrium electronic structure induced by the rotation of the magnetic moments [17,18,20]. In the case of the collinear antiferromagnet CuMnAs, understanding of the anisotropic magnetoresistance and magnetic anisotropy is crucially important for the design of memory devices based on the reorientation of the Néel vector and the interpretation of their electrical readout signal. Moreover, due to the predicted dependence of the electronic band structure on Néel vector orientation in CuMnAs and related materials [7,21], a significant crystalline AMR effect may be expected, i.e., a dependence of the electrical resistance on the directions of the current and the Néel vector with respect to crystalline symmetry [16].

Here, we demonstrate magnetic-field-induced spin rotation and spin-flop behavior in epitaxial films of tetragonal CuMnAs, using x-ray magnetic linear dichroism (XMLD) spectroscopy as well as integral magnetometry. XMLD is the dependence of the x-ray absorption cross section on the

---

relative orientation of the x-ray linear polarization and the spin axis [22]. Unlike x-ray magnetic circular dichroism (XMCD), XMLD is an even function of the magnetic moment, can be detected equally in ferromagnets and antiferromagnets, and is widely used for AF domain imaging [5,6,9,23,24]. We then show that the signature of the spin flop or spin reorientation can also be detected electrically. This allows us to determine the crystalline and noncrystalline contributions to the AMR in this material, of importance for interpreting and optimizing the electrical readout in AF memory devices.

II. SAMPLE GROWTH AND MAGNETIC CHARACTERIZATION

The tetragonal CuMnAs films, with thicknesses between 10 and 50 nm, were grown on GaP(001) substrates using molecular beam epitaxy. CuMnAs is lattice-matched to GaP through a 45° rotation, such that the CuMnAs [100] axis is aligned with the GaP [110] [25]. Previous characterizations using neutron diffraction as well as x-ray and optical techniques on similar samples have revealed a dependence of the magnetic anisotropy on film thickness [6,26,27]. For thin ($\leqslant 20$ nm) CuMnAs/GaP(001) layers, a uniaxial in-plane easy axis along the substrate [110] direction has been demonstrated [26,27], similar to well-known ferromagnet/III-V systems such as Fe/GaAs(001) [28]. Thicker films show a biaxial AF domain structure with easy axes along the CuMnAs [110] and [1$\bar{1}$0] axes [6].

Mn $L_{2,3}$-edge x-ray absorption spectroscopy measurements were performed on Beamline I06-1 at Diamond Light Source, at a sample temperature of 200 K. The samples showed negligible XMCD even at the highest field applied of 6 T, indicating very small canting of the magnetic moments due to their strong AF coupling. The XMLD measurements were performed with the x-ray beam and the external magnetic field both at 15° to the plane of the film [see Fig. 1(a), inset], with the x-ray linear polarization along the CuMnAs [010] in-plane direction (i.e., the substrate [1$\bar{1}$0] direction). The absorption spectra for a 20-nm film are shown in Fig. 1(a). A significant difference is observed between spectra obtained at low and high external magnetic fields, as shown by the difference spectrum in Fig. 1(a).

The difference spectrum in Fig. 1(a) is of comparable magnitude, relative to the absorption edge, to the XMLD spectrum previously observed in ferromagnetic Mn compounds [29,30]. Also, comparable spectra are observed when the absorption is detected with both total electron yield (probing depth $\sim$3 nm) and fluorescence yield (probing depth >10 nm, not shown), ruling out a pure surface effect. Figures 1(b) and 1(c) show the field dependence of the XMLD signal, defined here as the peak-to-peak of the difference between spectra obtained in a magnetic field and in zero field. Distinct behaviors are observed for 20- and 50-nm-thick CuMnAs films. For 20-nm CuMnAs, the XMLD signal shows a sharp onset at around 1.5 T and a plateau at around 2.5 T for the magnetic field projected along the [100] direction, while negligible XMLD is observed for the field projected along the [010] direction. For the 50-nm film, similar behavior is seen for both [100] and [010] directions, with an initial quadratic rise followed by saturation for fields above around 2 T.
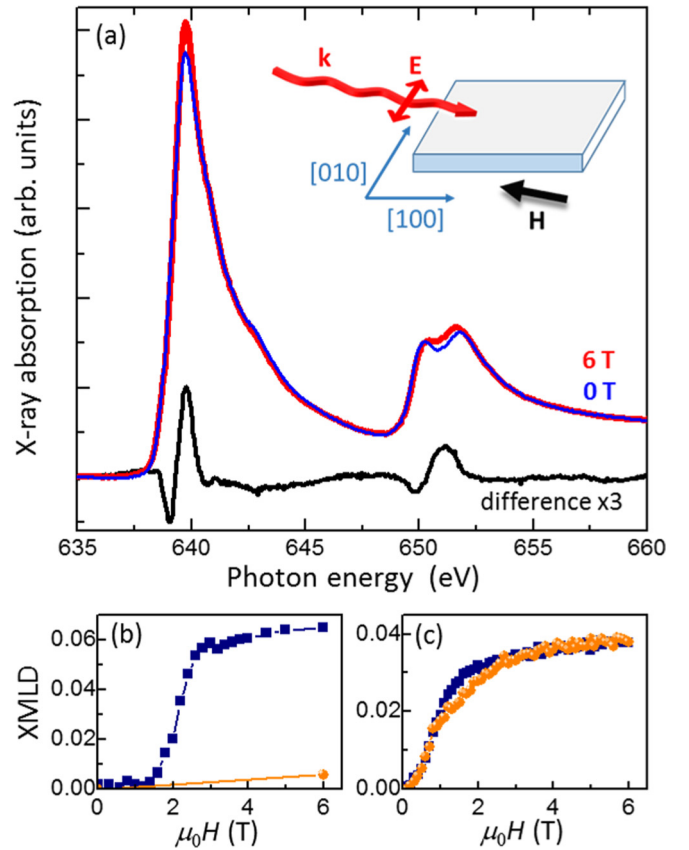

FIG. 1. (a) Mn $L_{2,3}$ x-ray absorption spectra measured in total electron yield for 20-nm CuMnAs, in zero field (blue), 6-T field (red), and the difference (black), at 200 K. The x-ray incidence **k** and the external magnetic field **H** are at 15° to the sample surface, while the x-ray linear polarization **E** is along the CuMnAs [010] in-plane axis, as illustrated in the inset. The CuMnAs [100] axis is projected along the beam direction. (a), (b) XMLD signal measured in fluorescence yield versus increasing magnetic field for (b) 20-nm and (c) 50-nm CuMnAs films. Blue squares and orange circles are for the in-plane projection of the field H_x along the [100] and [010] axes, respectively.

The observed behavior is consistent with the Néel vector reorientation expected for a system with competing uniaxial and biaxial magnetic anisotropies. For the thinner film with dominant uniaxial anisotropy, the **L** vector undergoes a spin-flop transition into an axis perpendicular to the applied magnetic field. In this experimental geometry, **L** is perpendicular to the x-ray polarization at low fields, and parallel to it at high fields, resulting in a spectral change due to XMLD. For the thicker film, biaxial magnetic anisotropy is dominant, resulting in a so-called continuous spin-flop transition [31] as the **L** vector rotates continuously into an axis perpendicular to the external field.

The XMLD hysteresis loop for a 10-nm CuMnAs film is shown in Fig. 2(a), for in-plane projection of the magnetic field along the [100] direction. At high magnetic fields, the XMLD signal is symmetric with respect to the field, as expected from its dependence on the square of the sublattice magnetic moment [22]. The hysteresis behavior observed in
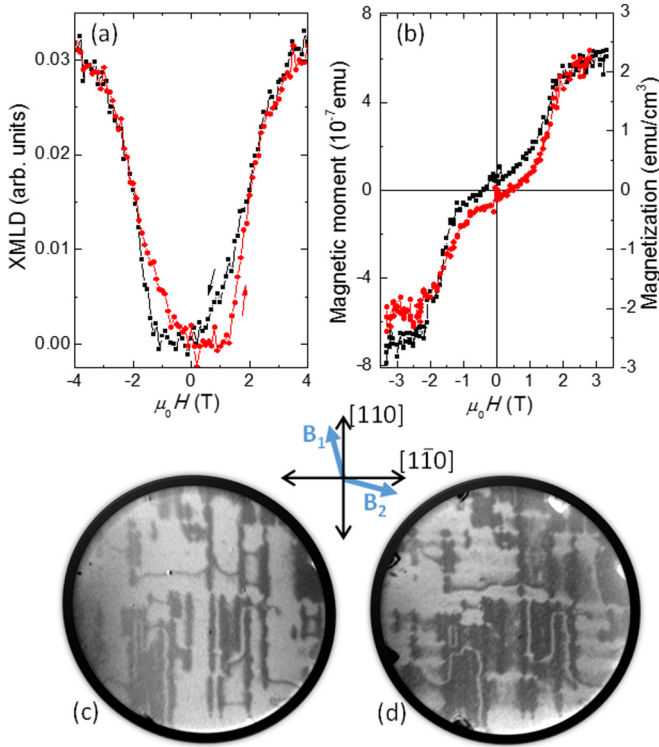
FIG. 2. (a) XMLD hysteresis loop, measured in fluorescence yield, for a 10-nm CuMnAs film at 200 K. (b) SQUID hysteresis loop for a 10-nm CuMnAs film at 2 K, after removal of the substrate diamagnetic signal. (c), (d) XPEEM images, with a 30-μm field-of-view, of the antiferromagnetic domain structure in a 50-nm CuMnAs film at room temperature. The sample is at remanence after applying 7-T magnetic fields in the directions B1 and B2 shown in the inset. Dark/light domains correspond to a Néel vector parallel/perpendicular to the x-ray polarization, which is along the CuMnAs [110] axis.

the vicinity of the spin-flop transition indicates the formation of multidomain states in the thin CuMnAs film [32].

To further confirm and quantify the spin-flop behavior, the field dependence of the magnetization $M(H)$ along the uniaxial easy axis of a 10-nm CuMnAs film was determined at 2 K using a Quantum Design MPMS superconducting quantum interference device (SQUID) magnetometry system [33]. To *in situ* compensate the much larger magnetic response of the GaP substrate, the sample was mounted between two abutting 8-cm-long strips cut from another (equivalent) 2-in. GaP wafer, and careful calibration procedures were performed [34]. The compensational sample holder assembled for these measurements is presented in Fig. 4(d) in Ref. [34]. The results [Fig. 2(b)] indicate a magnetization due to the spin canting of (2.0 ± 0.5) emu/cm^3 under 2-T field, where the uncertainty mostly arises from the subtraction of the substrate background signal. Given a local magnetic moment of $(3.6 \pm 0.2)\mu_B$ per Mn atom in tetragonal CuMnAs obtained from neutron diffraction [25], the fully saturated magnetization of the CuMnAs film is estimated to be (720 ± 40) emu/cm^2. Therefore, a canting angle of $\theta_{sf} \approx 0.2°$ is estimated from the trigonometric relation of the magnetization component at the spin-flop field. The exchange field is then estimated from

$\theta_{sf} = \cos(H/H_e)$ to be $\mu_0 H_e = (700 \pm 200)$ T. The spin-flop field $\mu_0 H_{sf} \approx 2$ T, therefore, corresponds to a magnetic anisotropy field of the order of $H_{sf}^2/H_e \approx 5$ mT.

Figures 2(c) and 2(d) show images of the antiferromagnetic domain configuration in a 50-nm CuMnAs film obtained using x-ray photoemission electron microscopy (XPEEM), in remanence after applying 7-T magnetic fields at approximately 15° from the CuMnAs [110] [Fig. 2(c)] and [1$\bar{1}$0] [Fig. 2(d)] biaxial easy axes. In both cases, the film is in a multidomain state after removing the external magnetic field, with a domain structure which is consistent with previous observations of similar CuMnAs films [6]. Similar features can be identified in each image, albeit with a significant remnant effect, i.e., a preponderance of light domains in Fig. 2(c) and dark domains in Fig. 2(d). This indicates that the magnetization process in the biaxial CuMnAs films likely proceeds through Néel vector reorientation within the multiple domains as well as through domain wall motion.

III. ANISOTROPIC MAGNETORESISTANCE

DC magnetotransport measurements were performed on Hall bar devices fabricated from the CuMnAs films. Figure 3 shows data for the 10-nm-thick CuMnAs film at 4 K, for L-shaped Hall bars with current channels along the [100], [010], [110], and [1$\bar{1}$0] crystalline directions. Optical micrographs of the devices are shown in Figs. 3(a) and 3(b). Magnetic fields were applied in the plane of the film at an angle θ to the current direction. Figures 3(c) and 3(d) show the normalized longitudinal component of the resistivity tensor ($[R_{xx} - R_{xx}(H = 0)]/R_{xx}(H = 0)$, where R_{xx} is the longitudinal resistance) as a function of the magnetic field. A steplike change in the resistance is observed between 1 and 2 T for fields applied along the easy axis [Fig. 3(c)], while a much weaker magnetoresistance is observed for fields perpendicular to the easy axis [Fig. 3(d)].

Figures 3(e) and 3(f) show the normalized transverse component of the resistivity tensor ($[R_{xy} - R_{xy}(H = 0)]/R_{sq}$, where R_{sq} is the sheet resistance of $\approx 20 \, \Omega$ per square at zero field). Again, a steplike change is observed for fields applied along the easy axis. For the longitudinal and transverse resistances, the steplike behavior is observed for current parallel/perpendicular and at 45°/225° to the magnetic field, respectively. This is consistent with the standard phenomenology of AMR [35]. Including terms dependent on the crystalline anisotropy in a single crystal with twofold and fourfold symmetry components, the longitudinal and transverse components of AMR can be written [36] as

$$\begin{aligned} AMR_{xx} &= (R_{xx} - R_{\text{ave}})/R_{\text{ave}} \\ &= C_I \cos(2\phi) + C_U \cos(2\psi) \\ &\quad + C_C \cos(4\psi) + C_{IC} \cos(4\psi - 2\phi), \end{aligned} \quad (1)$$

$$\begin{aligned} AMR_{xy} &= R_{xy}/R_{sq} \\ &= C_I \sin(2\phi) - C_{IC} \sin(4\psi - 2\phi), \end{aligned} \quad (2)$$

where ϕ and ψ are the angles of the magnetization (for a ferromagnet) or the Néel vector (for an AF material) with respect to the current direction and the [100] crystalline axis,
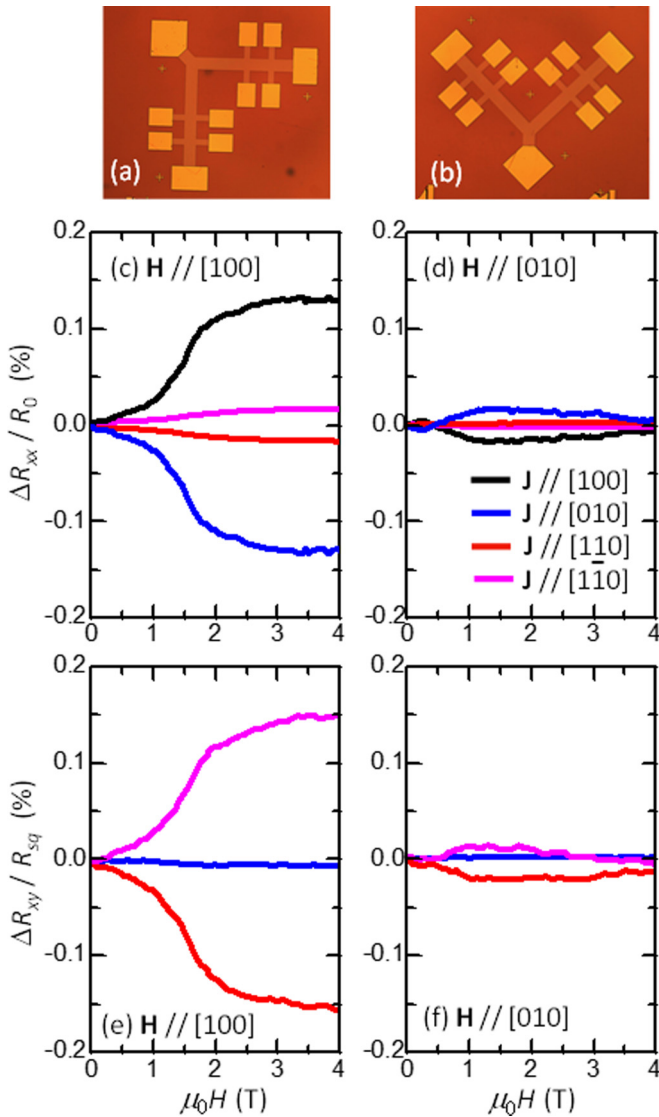
FIG. 3. (a), (b) Optical micrographs of the L-shaped Hall bar devices with current channels along (a) [100]/[010] and (b) [110]/[1$\bar{1}$0] crystalline directions. (c), (d) Longitudinal and (e), (f) transverse magnetoresistances for 10-nm-thick CuMnAs at 4 K, with the magnetic field increasing along the [100] (c,e) and [010] (d), (f) crystal axes, for various current directions indicated by the legend in panel (d).
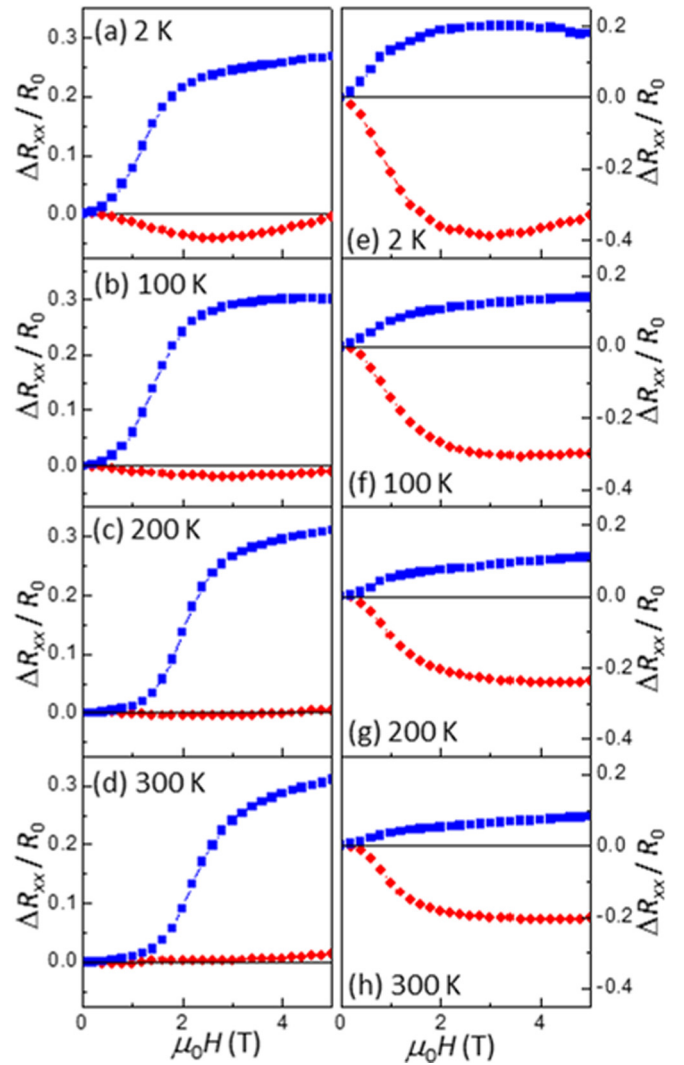

FIG. 4. Longitudinal magnetoresistances at 2, 100, 200, and 300 K for (a)–(d) 20-nm CuMnAs films and (e)–(h) 50-nm CuMnAs films. The current is along the [100] direction, and the magnetic field is increasing along the [100] (blue squares) and [010] (red circles) directions.

respectively. R_{ave} is the longitudinal resistance averaged over a full rotation in the plane of the film. C_I, C_U, C_C, and C_{IC} are phenomenological AMR coefficients corresponding to a noncrystalline term, twofold and fourfold crystalline terms, and a crossed crystalline/noncrystalline term, respectively.

The longitudinal magnetoresistance for 20- and 50-nm CuMnAs films at various temperatures are shown in Fig. 4, for current along the [100] direction and magnetic fields along the [100] and [010] directions. Uniaxial spin-flop behavior and continuous spin reorientation are observed for the 20- and 50-nm films, respectively, consistent with the XMLD field dependence shown in Figs. 1(b) and 1(c). For the 20-nm film, with decreasing temperature, the spin-flop field decreases, and a small negative magnetoresistance is observed for the

field along [010]. This indicates an increasing importance of the biaxial magnetic anisotropy with decreasing temperature, consistent with the expected strong dependence of biaxial anisotropy fields on sublattice magnetization [37].

The longitudinal resistance versus angle θ is shown in Fig. 5(a), for a 10-nm CuMnAs film at 4 K with magnetic fields comparable or smaller than H_{sf}. The current is along the [010] direction. With a decreasing external field, the oscillations in the resistance become smaller and more anharmonic. This can be ascribed to the increasing importance of the magnetic anisotropy, resulting in the Néel vector only partially reorienting from its zero-field direction. The observed behavior can be simulated within a simple single-domain model including a uniaxial magnetic anisotropy. This simplified model agrees well with the observed dependence on both the magnitude and the direction of the external magnetic field, including the appearance of additional features in the angle dependence for $\mu_0 H = 1$ T, as shown in Fig. 5(b). The
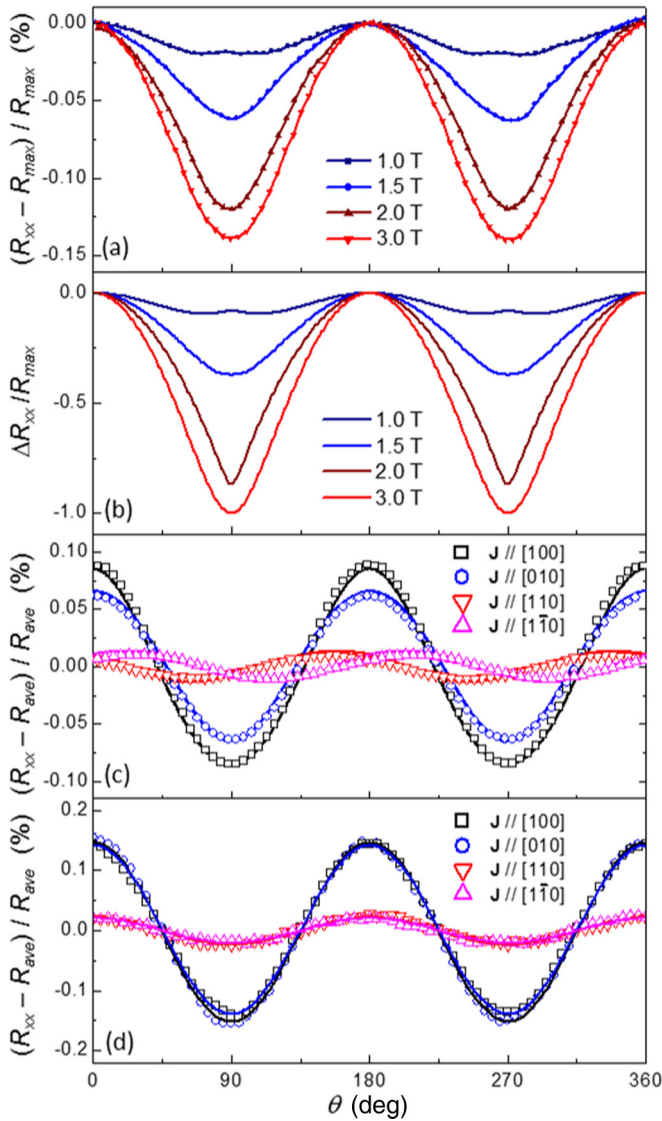
FIG. 5. Resistance vs angle θ between the magnetic field and the current directions at 4 K. (a) 10-nm CuMnAs: current along the [010] direction; magnetic fields of magnitude 1.0, 1.5, 2.0, and 3.0 T. (b) Calculated anisotropic magnetoresistance for a uniaxial antiferromagnet with a Gaussian distribution of spin-flop fields centered on 1.6 T with a standard deviation of 0.7 T. (c) 10-nm CuMnAs: current along the [100], [010], [110], and [1$\bar{1}$0] crystal directions; magnetic field of magnitude 5 T. (d) 50-nm CuMnAs: current along the [100], [010], [110], and [1$\bar{1}$0] crystal directions; magnetic field of magnitude 5 T. The lines in panels (c) and (d) are fits as described in the text.

FIG. 6. (a), (b) Magnetoresistance for 10-nm CuMnAs under high magnetic fields at 4 K, for current along the [100] and [010] directions, and applied magnetic field perpendicular and parallel to the current. (c) Difference between the magnetoresistances for parallel and perpendicular orientations of current and magnetic field, for currents along the [100] and [010] directions. (d) Angle dependence of resistance for current along [010] at 13 T (squares) and for current along [100] at 14 T (circles). The lines are fits of the form $(a\cos 2\theta + b\cos 4\theta)$, with a and b as fit parameters.

Gaussian distribution of spin-flop fields used in this simplified model may reflect the role of domain walls and structural defects as well as biaxial magnetic anisotropy, all of which can give rise to a broadening of the spin-flop transition.

At higher fields, the longitudinal resistance follows a $\cos 2\theta$ dependence, as expected from Eq. (1) with $C_I, C_U, C_{IC} \gg C_C$ when the Néel vector aligns fully perpendicular to the field (i.e., $\phi = \theta$). However, as shown in Figs. 5(c) and 5(d) for 10- and 50-nm films, the observed $R_{xx}(\theta)$ depends strongly on the direction of the current,
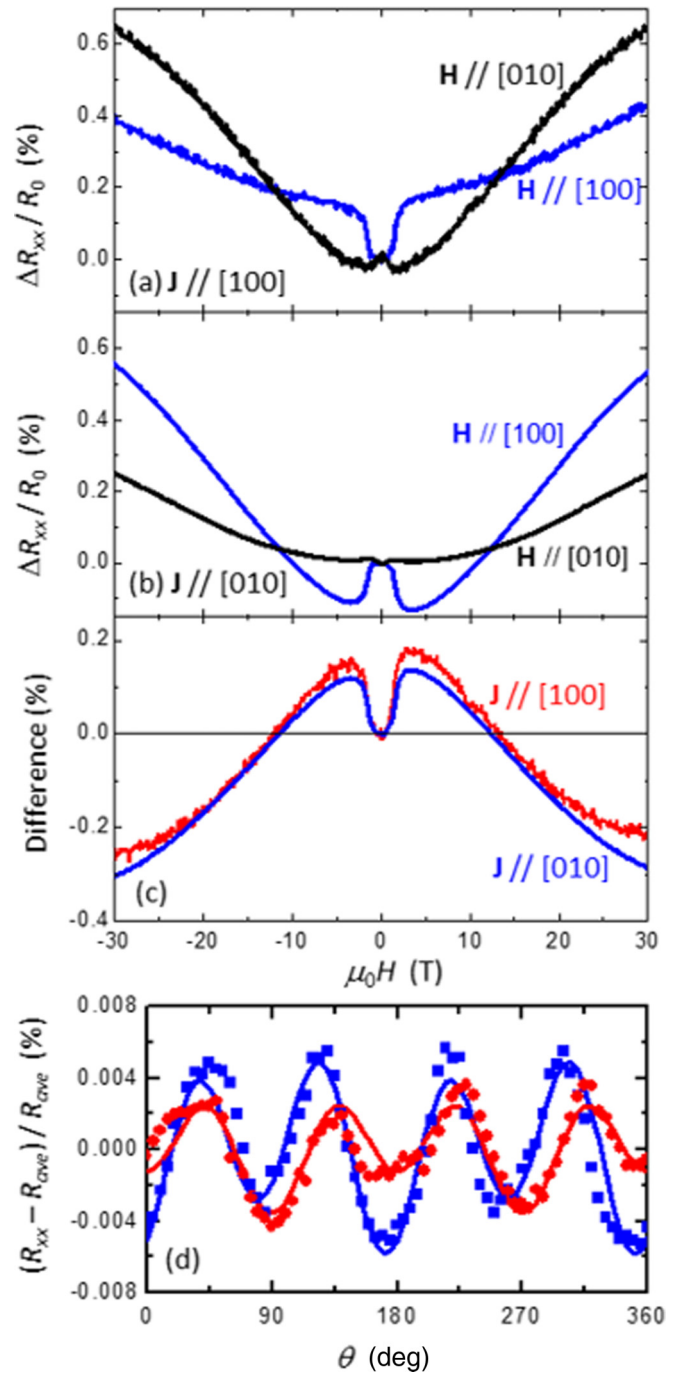
demonstrating the importance of the crystalline contributions to the AMR. For currents along the [110] and [1$\bar{1}$0] directions, the AMR is much reduced, and for the 10-nm film, it is phase shifted by around $\pm 25°$. By fitting the field rotation data

we obtain the AMR coefficients $C_I = (4.1 \pm 0.1) \times 10^{-4}$, $C_U = (1.0 \pm 0.2) \times 10^{-4}$, and $C_{IC} = (3.5 \pm 0.1) \times 10^{-4}$ for the 10-nm film, and $C_I = (8.3 \pm 0.1) \times 10^{-4}$, $C_U \approx 0$, and $C_{IC} = (6.2 \pm 0.1) \times 10^{-4}$ for the 50-nm film. In both cases the C_{IC} term is comparable in magnitude to the C_I term. Therefore, these two terms largely cancel each other out for current along the [110] and [1$\bar{1}$0] directions, and the AMR is strongly suppressed. The non-negligible uniaxial term C_U for the 10-nm film accounts for the difference in the AMR magnitude between the [100] and [010] current directions, and the phase shift for the [110] and [1$\bar{1}$0] directions. It is likely that this uniaxial crystalline AMR has the same origin as the uniaxial magnetic anisotropy, giving rise to the spin flop, e.g., anisotropic growth initiated at the III-V semiconductor surface.

The magnetoresistance at higher magnetic fields is shown in Figs. 6(a)–6(c), for a 10-nm CuMnAs film at 4 K. In addition to the AMR, a positive magnetoresistance is observed for all directions of magnetic field and current. Moreover, the highest resistance occurs when the current and the magnetic field are perpendicular at high fields. This is opposite to the case at low fields where the highest resistance is when the field and the current are coaxial. We ascribe the high field behavior to a geometrical magnetoresistance effect, not directly related to the magnetic order, which is commonly observed in thin conducting films [38]. Field rotation measurements at the crossover between low-field and high-field regimes, shown in Fig. 6(d), indicate a weak AMR with a dominant fourfold symmetry. For the rotation data at 5 T [Fig. 5(c)], the fourfold AMR term C_C could not be distinguished due to the much larger two-fold AMR terms [see Eq. (1)]. In the crossover regime [Fig. 6(d)], the twofold AMR terms are nearly canceled by the geometrical magnetoresistance effect. The remaining fourfold AMR has resistance minima for magnetic fields along the $\langle 110 \rangle$ crystalline axes.

IV. DISCUSSION AND SUMMARY

The magnetotransport effects shown in Figs. 3 to 6 provide a practical experimental tool for the determination of spin reorientation in antiferromagnetic domains and magnetic anisotropies in thin CuMnAs AF films. They also provide a direct measurement of the AMR coefficients and point to the importance of crystalline AMR terms in these epitaxial AF materials. The measured AMR corresponds to a fraction of a percent of the sheet resistance, comparable to the size of the electrical readout signals observed in the first demonstrations of current-induced switching in CuMnAs microdevices [4–6].

More recently, resistive signals of the order of 10–100% have been observed in the same CuMnAs films as used in the present study. These signals are switchable with unipolar current pulses or polarization-independent optical pulses, even in magnetic fields much larger than H_{sf} [39]. The present study provides confirmation that the large switching signals are not linked to a net reorientation of the Néel vector and the corresponding AMR. A recent magnetostatic imaging study has instead linked the large unipolar switching signal to a current-induced fragmentation to nanoscale AF domain textures, and subsequent relaxation towards an equilibrium domain configuration [40]. In principle, however, so far unidentified structural effects may also contribute or even govern these large effects. Future systematic experiments in magnetic fields might, therefore, contribute not only to our understanding of the current-induced Néel vector switching and AMR but also to our understanding of these high-resistive switching signals in CuMnAs.

[1] T. Jungwirth, X. Marti, P. Wadley, and J. Wunderlich, Antiferromagnetic spintronics, Nat. Nanotechnol. **11**, 231 (2016).

[2] V. Baltz, A. Manchon, M. Tsoi, T. Moriyama, T. Ono, and Y. Tserkovnyak, Antiferromagnetic spintronics, Rev. Mod. Phys. **90**, 015005 (2018).

[3] J. Zelezny, H. Gao, K. Vyborny, J. Zemen, J. Masek, A. Manchon, J. Wunderlich, J. Sinova, and T. Jungwirth, Relativistic Néel-Order Fields Induced by Electrical Current in Antiferromagnets, Phys. Rev. Lett. **113**, 057201 (2014).

[4] P. Wadley, B. Howells, J. Zelezny, C. Andrews, V. Hills, R. P. Campion, V. Novak, K. Olejnik, F. Maccherozzi, S. S. Dhesi *et al.*, Electrical switching of an antiferromagnet, Science **351**, 587 (2016).

[5] M. J. Grzybowski, P. Wadley, K. W. Edmonds, R. Beardsley, V. Hills, R. P. Campion, B. L. Gallagher, J. S. Chauhan, V. Novak, T. Jungwirth, F. Maccherozzi, and S. S. Dhesi, Imaging Current-Induced Switching of Antiferromagnetic Domains in CuMnAs, Phys. Rev. Lett. **118**, 057701 (2017).

[6] P. Wadley, S. Reimers, M. J. Grzybowski, C. Andrews, M. Wang, J. S. Chauhan, B. L. Gallagher, R. P. Campion, K. W. Edmonds, S. S. Dhesi, F. Maccherozzi, V. Novak, J. Wunderlich, and T. Jungwirth, Current polarity-dependent manipulation of antiferromagnetic domains, Nat. Nanotechnol. **13**, 362 (2018).

[7] S. Y. Bodnar, L. Šmejkal, I. Turek, T. Jungwirth, O. Gomonay, J. Sinova, A. A. Sapozhnik, H.-J. Elmers, M. Klaui, and M.

Jourdan, Writing and reading antiferromagnetic Mn_2Au by Néel spin-orbit torques and large anisotropic magnetoresistance, Nat. Commun. **9**, 348 (2018).

[8] M. Meinert, D. Graulich, and T. Matalla-Wagner, Electrical Switching of Mn_2Au and the Role of Thermal Activation, Phys. Rev. Appl. **9**, 064040 (2018).

[9] S. Y. Bodnar, M. Filianina, S. P. Bommanaboyena, T. Forrest, F. Maccherozzi, A. A. Sapozhnik, Y. Skourski, M. Klaui, and M. Jourdan, Imaging of current induced Néel vector switching in antiferromagnetic Mn_2Au, Phys. Rev. B **99**, 140409(R) (2019).

[10] X. Z. Chen, X. F. Zhou, R. Cheng, C. Song, J. Zhang, Y. C. Wu, Y. Ba, H. B. Li, Y. M. Sun, Y. F. You, Y. G. Zhao, and F. Pan, Electric field control of Néel spin-orbit torque in an antiferromagnet, Nat. Mater. **18**, 931 (2019).

[11] A. B. Shick, S. Khmelevskyi, O. N. Mryasov, J. Wunderlich, and T. Jungwirth, Spin-orbit coupling induced anisotropy effects in bimetallic antiferromagnets: A route towards antiferromagnetic spintronics, Phys. Rev. B **81**, 212409 (2010).

[12] B. G. Park, J. Wunderlich, X. Marti, V. Holy, Y. Kurosaki, M. Yamada, H. Yamamoto, A. Nishide, J. Hayakawa, H. Takahashi, A. B. Shick, and T. Jungwirth, A spin-valve-like magnetoresistance of an antiferromagnet-based tunnel junction, Nat. Mater. **10**, 347 (2011).

[13] Y. Y. Wang, C. Song, B. Cui, G. Y. Wang, F. Zeng, and F. Pan, Room-Temperature Perpendicular Exchange Coupling and Tunneling Anisotropic Magnetoresistance in an Antiferromagnet-Based Tunnel Junction, Phys. Rev. Lett. **109**, 137201 (2012).

[14] X. Marti, I. Fina, C. Frontera, J. Liu, P. Wadley, Q. He, R. J. Paull, J. D. Clarkson, J. Kudrnovský, I. Turek, J. Kuneš, D. Yi, J.-H. Chi, C. T. Nelson, L. You, E. Arenholz, S. Salahuddin, J. Fontcuberta, T. Jungwirth, and R. Ramesh, Room-temperature antiferromagnetic memory resistor, Nat. Mater. **13**, 367 (2014).

[15] D. Kriegner, K. Vyborny, K. Olejnik, H. Reichlova, V. Novak, X. Marti, J. Gazquez, V. Saidl, P. Nemec, V. V. Volobuev, G. Springholz, V. Holy, and T. Jungwirth, Multiple-stable anisotropic magnetoresistance memory in antiferromagnetic MnTe, Nat. Commun. **7**, 11623 (2016).

[16] D. Kriegner, H. Reichlova, J. Grenzer, W. Schmidt, E. Ressouche, J. Godinho, T. Wagner, S. Y. Martin, A. B. Shick, V. V. Volobuev, G. Springholz, V. Holy, J. Wunderlich, T. Jungwirth, and K. Vyborny, Magnetic anisotropy in antiferromagnetic hexagonal MnTe, Phys. Rev. B **96**, 214418 (2017).

[17] I. Fina, X. Marti, D. Yi, J. Liu, J. H. Chu, C. Rayan-Serrao, S. Suresha, A. B. Shick, J. Zelezny, T. Jungwirth, J. Fontcuberta, and R. Ramesh, Anisotropic magnetoresistance in an antiferromagnetic semiconductor, Nat. Commun. **5**, 4671 (2014).

[18] C. Wang, H. Seinige, G. Cao, J.-S. Zhou, J. B. Goodenough, and M. Tsoi, Anisotropic Magnetoresistance in Antiferromagnetic Sr_2IrO_4, Phys. Rev. X **4**, 041034 (2014).

[19] R. Galceran, I. Fina, J. Cisneros-Fernandez, B. Bozzo, C. Frontera, L. Lopez-Mir, H. Deniz, K. W. Park, B. G. Park, L. Balcells, X. Marti, T. Jungwirth, and B. Martinez, Isothermal anisotropic magnetoresistance in antiferromagnetic metallic IrMn, Sci. Rep. **6**, 35471 (2016).

[20] C. Lu, B. Gao, H. Wang, W. Wang, S. Yuan, S. Dong, and J.-M. Liu, Revealing controllable anisotropic magnetoresistance in spin orbit coupled antiferromagnet Sr_2IrO_4, Adv. Funct. Mater. **28**, 1706589 (2018).

[21] L. Smejkal, J. Zelezny, J. Sinova, and T. Jungwirth, Electric Control of Dirac Quasiparticles by Spin-Orbit Torque in an Antiferromagnet, Phys. Rev. Lett. **118**, 106402 (2017).

[22] G. van der Laan, B. T. Thole, G. A. Sawatzky, J. B. Goedkoop, J. C. Fuggle, J.-M. Esteva, R. Karnatak, J. P. Remeika, and H. A. Dabkowska, Experimental proof of magnetic x-ray dichroism, Phys. Rev. B **34**, 6529 (1986).

[23] A. Scholl, J. Stohr, J. Luning, J. W. Seo, J. Fompyrine, H. Siegwart, J. P. Loquet, F. Nolting, S. Anders, E. E. Fullerton, M. R. Scheinfein, and H. A. Padmore, Observation of antiferromagnetic domains in epitaxial thin films, Science **287**, 1014 (2000).

[24] F. Nolting, A. Scholl, J. Stohr, J. W. Seo, J. Fompeyrine, H. Siegwart, J. P. Locquet, S. Anders, J. Luning, E. E. Fullerton, M. F. Toney, M. R. Scheinfein, and H. A. Padmore, Direct observation of the alignment of ferromagnetic spins by antiferromagnetic spins, Nature (London) **405**, 767 (2000).

[25] P. Wadley, V. Novak, R. P. Campion, C. Rinaldi, X. Marti, H. Reichlova, J. Zelezny, J. Gazquez, M. A. Roldan, M. Varela *et al.*, Tetragonal phase of epitaxial room-temperature antiferromagnet CuMnAs, Nat. Commun. **4**, 2322 (2013).

[26] P. Wadley, V. Hills, M. R. Shahedkhah, K. W. Edmonds, R. P. Campion, V. Novak, B. Ouladdiaf, D. Khalyavin, S. Langridge, V. Saidl, P. Nemec, A. W. Rushforth, B. L. Gallagher, S. S. Dhesi, F. Maccherozzi, J. Zelezny, and T. Jungwirth, Antiferromagnetic structure in tetragonal CuMnAs thin films, Sci. Rep. **5**, 17079 (2015).

[27] V. Saidl, P. Nemec, P. Wadley, V. Hills, R. P. Campion, V. Novak, K. W. Edmonds, F. Maccherozzi, S. S. Dhesi, B. L. Gallagher, F. Trojanek, J. Kunes, J. Zelezny, P. Maly, and T. Jungwirth, Optical determination of the Néel vector in a CuMnAs thin-film antiferromagnet, Nat. Photonics **11**, 91 (2017).

[28] G. Bayreuther, J. Premper, M. Sperl, and D. Sander, Uniaxial magnetic anisotropy in Fe/GaAs(001): Role of magnetoelastic interactions, Phys. Rev. B **86**, 054418 (2012).

[29] A. A. Freeman, K. W. Edmonds, G. van der Laan, N. R. S. Farley, T. K. Johal, E. Arenholz, R. P. Campion, C. T. Foxon, and B. L. Gallagher, Giant anisotropy in x-ray magnetic linear dichroism in (Ga,Mn)As, Phys. Rev. B **73**, 233303 (2006).

[30] M. Meinert, J. M. Schmalhorst, C. Klewe, G. Reiss, E. Arenholz, T. Bohnert, and K. Nielsch, Itinerant and localized magnetic moments in ferrimagnetic Mn_2CoGa thin films probed by x-ray magnetic linear dichroism: Experiment and *ab initio* theory, Phys. Rev. B **84**, 132405 (2011).

[31] K. Kliemt, M. Hofmann-Kliemt, K. Kummer, F. Yakhou-Harris, C. Krellner, and C. Geibel, $GdRh_2Si_2$: An exemplary tetragonal system for antiferromagnetic order with weak in-plane anisotropy, Phys. Rev. B **95**, 134403 (2017).

[32] A. N. Bogdanov, A. V. Zhuravlev, and U. K. Rossler, Spin-flop transition in uniaxial antiferromagnets: Magnetic phases, reorientation effects, and multidomain states, Phys. Rev. B **75**, 094425 (2007).

[33] M. Sawicki, W. Stefanowicz, and A. Ney, Sensitive SQUID magnetometry for studying nano-magnetism, Semicond. Sci. Technol. **26**, 064006 (2011).

[34] K. Gas and M. Sawicki, *In situ* compensation method for high-precision and high-sensitivity integral magnetometry, Meas. Sci. Technol. **30**, 085003 (2019).

[35] T. R. McGuire and R. I. Potter, Anisotropic magnetoresistance in ferromagnetic 3d alloys, IEEE Trans. Magn. **11**, 1018 (1975).

[36] A. W. Rushforth, K. Vyborny, C. S. King, K. W. Edmonds, R. P. Campion, C. T. Foxon, J. Wunderlich, A. C. Irvine, P. Vasek, V. Novak, K. Olejnik, J. Sinova, T. Jungwirth, and B. L. Gallagher, Anisotropic Magnetoresistance Components in (Ga,Mn)As, Phys. Rev. Lett. **99**, 147207 (2007).

[37] H. B. Callen and E. Callen, The present status of the temperature dependence of magnetocrystalline anisotropy and the l(l+1)/2 power law, J. Phys. Chem. Solids **27**, 1271 (1966).

[38] A. B. Pippard, *Magnetoresistance in Metals* (Cambridge University, Cambridge, England, 1989).

[39] Z. Kaspar, M. Surynek, J. Zubac, F. Krizek, V. Novak, R. P. Campion, M. S. Wornle, P. Gambardella, X. Marti, P. Nemec, P. Wadley, J. Wunderlich, T. Jungwirth, and K. Olejnik, High resistive unipolar-electrical and fs-optical switching in a single-layer antiferromagnetic memory, arXiv:1909.09071.

[40] M. S. Wornle, P. Welter, Z. Kaspar, K. Olejnik, V. Novak, R. P. Campion, P. Wadley, T. Jungwirth, C. L. Degen, and P. Gambardella, Current-induced fragmentation of antiferromagnetic domains, arXiv:1912.05287.